Icarus 424 (2024) 116285

Contents lists available at ScienceDirect

Icarus

journal homepage: www.elsevier.com/locate/icarus

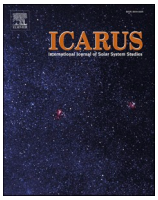

Identification and preliminary characterisation of signals recorded by instrument for lunar seismic activity at the Chandrayaan 3 landing site

J. John *, V. Thamarai, Teena Choudhary, M.N. Srinivasa, Ashwini Jambhalikar, M.S. Giridhar, Madan Mohan Mehra, Mayank Garg, K.V. Shila, Krishna Kummari, S.P. Karantha, Kalpana Arvind, K.V. Sriram

Laboratory for Electro-Optics Systems (LEOS), Indian Space Research Organisation (ISRO), Peenya 1st Stage, 1st Cross, Bengaluru 560058, India

ARTICLE INFO

Keywords:
Chandrayaan 3
Short period seismometer
MEMS
Seismic signals

ABSTRACT

The science objective of the Instrument for Lunar Seismic Activity (ILSA) is to study the seismicity at the landing site of the Indian lunar mission, the Chandrayaan 3. It also aimed at demonstrating the capability of devices based on silicon micromachining technology to survive and operate in planetary missions and environments. The Chandrayaan 3 mission had a lander and a rover together carrying five different scientific instruments. ILSA was placed on the lunar surface and had six accelerometers in it. It was operated during the lunar day from 24 August 2023 to 4 September 2023. This paper presents the summary of observations made on 190 h of data recorded by ILSA. We have identified more than 250 distinct signals of which about 200 signals are correlated to known activities involving the physical movements of the rover or the operation of science instruments. This paper presents our approach in the preliminary characterisation and cataloguing of the events based on their temporal properties and spectral contents. It will also act a guide for the future researchers to search, identify and analyse the records made by ILSA.

1. Introduction

Chandrayaan 3 is the first ever mission to soft-land at the south polar region of the Moon with the landing site at 69.37^{O} S and 32.32^{O} E. The actual location of landing is well within the safe grid of the identified prime landing site with area 4 km × 2.4 km (Amitabh et al., 2023; Durga Prasad et al., 2023). The mission had a lander named *Vikram* and a rover named *Pragyaan* together carrying five major science instruments with multiple objectives. The Instrument for Lunar Seismic Activity had the objective of studying the seismicity at the landing site by recording the ground acceleration along the vertical and two horizontal directions which are mutually perpendicular to each other.

The seismicity of the lunar equatorial region has been well studied using the data provided by the multiple instruments of the Apollo lunar seismic network. These instruments were installed by astronauts during several missions from 1969 to 1972 and continued to generate data until 1977 (Gary et al., 2024; Robert et al., 2024; Lognonne and Johnson, 2015; Nakamura et al., 1982). There had been passive and active seismic profiling experiments. Detailed studies by various authors have consolidated and classified different event types as (i) Deep quakes (ii) Shallow quakes (iii) Impacts (iv) Thermal quakes (Nakamura, 1978; Nakamura, 2005; Nakamura et al., 1979; Duennebier and Sutton, 1974a; Oberst and Nakamura, 1987; Civilini et al., 2023). Several types of instruments namely long period seismometers, short period seismometers and geophones were employed to record the active and passive events. The data analysis by various authors have provided insights into planetary seismology. After the Apollo era, there were no major landing missions to Moon for about four decades. The Chang'e 3 landed in 2013 near Mare Imbrium 44.12^{O} N, 19.51^{O} W. Subsequently, Chang'e 4 landed at the far side of the Moon for the first time at 45.44^{O} S, 177.59^{O} E in the year 2019. Neither of these landers did carry seismic instruments. ILSA is the first instrument since the Apollo era to record ground accelerations on the Moon. They are the first ever signals obtained from an instrument placed at the lunar polar region. An awareness on the seismic background noise at this region is of great interest to researchers conceptualizing a lunar base and planning to conduct experiments like Lunar Gravity Wave Antenna detectors (Harms, 2022) in future. The instrument is first of its kind on the Moon as it employs sensing elements based on silicon micro machining technology, also called Micro Electro Mechanical Systems (MEMS) technology. Fig. 1

* Corresponding author.
E-mail address: jjohn@leos.gov.in (J. John).

https://doi.org/10.1016/j.icarus.2024.116285
Received 13 March 2024; Received in revised form 22 August 2024; Accepted 27 August 2024
Available online 29 August 2024

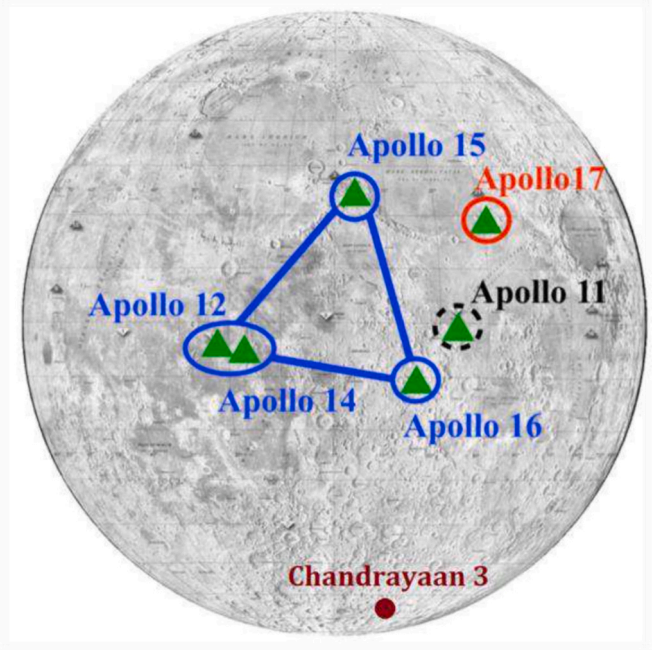

Fig. 1. The landing sites of Apollo and Chandrayaan 3 missions showing the locations where seismic data is recorded from Moon. A marker is introduced in the image from (Nunn et al., 2020) to represent Chandrayaan 3 landing site. *(With author's permission)*.

shows the locations on Moon where seismic data were recorded until 4 September 2023. Here a marker is added to the image provided in (Nunn et al., 2020) to indicate the location of Chandrayaan 3 landing site.

Apart from the Moon, the most successful seismic studies from a planetary body are from the Mars. The InSight mission recorded more than 1000 seismic events providing valuable data. The Seismic Experiment for Internal Structure instrument comprised of a three-axis very broad band seismometer and a three-axis short period seismometer. The details of the instrument construction, observations and the guide to process the signals are published in detail (Knapmeyer-Endrun and Kawamura, 2020; Lognonne et al., 2019; John et al., 2021). The short period seismometer in this experiment also employs a sensing element realized using silicon micromachining technology as in the case of ILSA. Other attempts, though not completely successful, are the instruments flown with the Venera missions to the Venus (Sanfomaliti et al., 1982) and the Viking missions to the Mars (Lorenz and Nakamura, 2013).

This paper presents a brief overview of the construction and working of ILSA and the details of its operation on the Moon. A preliminary analysis of the handpicked records and the approach developed for cataloguing them for future references and studies are also discussed.

2. Instrument details

ILSA consists of a cluster of six accelerometers with the sensing elements fabricated from single crystal silicon wafer employing MEMS technology. There are two types of sensors designated as coarse range and fine range sensors and are classified based on their sensitivity and resolution capabilities. The sensors are spring-mass systems that deflect in response to external acceleration obeying the classical spring equation. They are provided with comb electrodes interdigitated with another set of fixed electrodes. The construction of the sensing element leads to a change in gap between the electrodes upon the deflection of the proof mass which in turn results in a change in the associated capacitance. The sensor has Silicon-on-Glass architecture (SoG). The readout electronics is open loop by design. The noise equivalent acceleration of coarse range sensor is of the order of 10 μg, where 'g' is 9.8 ms^{-2}. The fine range sensor is designed to resolve sub μg levels of acceleration and has a bandwidth of around 50 Hz. The coarse range and fine range sensors had dynamic range of ±0.5 g and ± 15 mg (1 mg = 10^{-3} g), respectively. Both sensor structures are identical by construction, but differ in their mechanical and electrical sensitivities, proof mass dimensions, Brownian Noise Equivalent Acceleration and the capacitance conversion circuits. The coarse range sensor employs capacitance to digital conversion using a commercially available Integrated Circuit. The fine range sensor performs capacitance to voltage conversion followed by amplification using discrete components in die form. The sensing elements and the front-end readout electronics are packaged in a hybrid microcircuit package (HMC). Three HMCs are mounted in a mechanical housing orthogonal to each other to pick up signals along X, Y and Z directions of which the Z sensor has its sensitive axis along the vertical direction. This housing also contains a part of the electronics including the FPGA that generates the clock drives for the readout circuit, analog to digital converters and signal conditioning circuits before communicating the data to the data handling unit of the lander. The instrument had a size of 170 mm × 170 mm × 72 mm, weighed 1.8 kg and consumed around 4 W power. Photographs containing the MEMS sensors, HMCs and ILSA package are shown in Fig. 2.

The power supply for ILSA was sourced from a custom designed DC-DC converter mounted within the lander. This ensured the physical separation of the instrument from its power source. The 1.7 m long harness cable of the instrument included the power and data lines. More details on the design of the instrument and the performance specifications were published earlier (John et al., 2020).

3. ILSA operation on moon

Chandrayaan 3 landed on the Moon on 23 August 2023. ILSA was mounted at the central portion of the deployable ramp through which the rover rolled out from the lander to the lunar surface. The instrument was interfaced to the ramp using a mechanical structure having a Hold Down and Release Mechanism (HDRM) and the coiled harness cables in it. The HDRM had Shape Memory Alloy based Frangibolt actuators that detached the instrument from the ramp before its deployment to lunar surface. The mechanism assembly was provided with Kevlar threads wound and guided through two pairs of pulleys. The ends of the threads were tethered to the corners of the instrument. The gravity-assisted deployment was controlled by the motorized unwinding of the threads via the grooves of the pulleys. ILSA was powered on during its deployment process. Fig. 3 shows the signal recorded by the coarse range sensors during the deployment. There are three distinct parts in the plots along each axis. The first 25 s shows the output from the instrument after its detachment from the ramp but before the initiation of the deployment operation. The steady offset in the output of each sensor corresponds to the component of lunar gravity acting along the sensitive axis. The X and Z sensors experienced one component of the gravity vector acting along their sensitive axes. For the Y sensor, the gravity components were along its cross-axis directions. During the next 50 s, the instrument was getting deployed and the process induced high frequency vibrations as recorded along all the three directions. The third part of the graph shows the output offset after the placement of the instrument on the lunar surface. This signature was obtained during the pre-flight deployment trials at the laboratory. The magnitude of the offset in output of the coarse range sensors were used to estimate the tilt of placement of the instrument with respect to the local gravity vector. Some degree of tilt was expected due to the nature of the local terrain or the possibility of placement on features that can cause non-flat orientation of the instrument on the uneven lunar terrain. The design included a tilt correction method where an offset up to 30^{O} could be compensated using electrical signals generated within the instrument. The correction process could be achieved by sending commands from the ground. The instrument after its placement was measured to have a tilt around 24^{O}, 26^{O} and -14^{O}, respectively along X, Y and Z directions.

Fig. 2. Photographs showing the fine range and coarse range MEMS sensor chips (a), the 25 mm × 100 mm HMC package (b) and the 170 mm × 170 mm × 72 mm ILSA package with the harness cable (c).

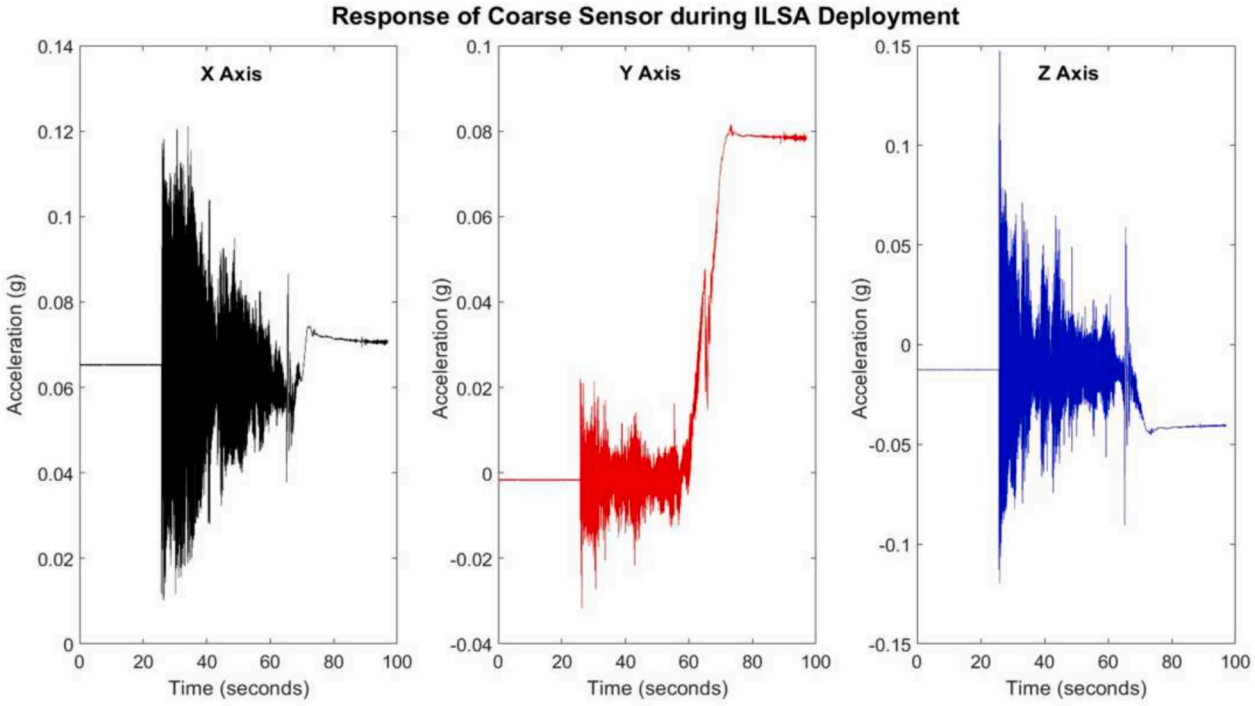

Fig. 3. Output recorded by the coarse range sensors during the deployment of ILSA. The initial offset, the vibration of the instrument during the deployment and the final offset confirms the expected sequence of operations.

These were compensated and ILSA was brought to its linear range of operation before the beginning of its normal operation mode on 24 August 2023 at 10:22:23 UTC. No special technique was incorporated to ensure a pre-defined orientation of ILSA during its placement on the lunar surface. However, due to the orientation of its mounting and the method of deploying, the sensitive axis of X sensor would be aligned to the direction of motion of the rover as it comes out of the ramp. ILSA was placed on the lunar surface near the lander as visible in the photograph shown in Fig. 4, which was taken by the navigation camera of the rover.

The instrument was operated continuously until 2 September 2023, 17:48:30 UTC. After switching off, it was stowed back as part of preparations for the 'hop experiment' during which the lander was relocated to a new position approximately 50 cm away from the initial site. The instrument was deployed again and it had a near-flat placement. The output from all the three axes were in the linear operating range and the electronic tilt correction was not carried out. The identical nature of signals recorded by ILSA during the insertion of the probe of the Chandra's Surface Thermophysical Experiment (ChaSTE) at both the locations confirm the integrity of signals captured under flat and tilt-corrected operation conditions. At the new location, ILSA recorded data from 02:38:58 UTC on 3 September to 01:47:11 UTC on 4 September 2023.

The instrument operated on the lunar surface for a total of about 218 h of which 190 h of data are available. This paper reports the preliminary observations made during the first evaluation of the records.

4. Temperature variations

During its operation at the landing site, ILSA experienced a wide range of temperature variation as recorded by the sensors in it. The instrument was operated during a lunar day where the sun elevation angle had changed steadily. However, the variation in temperature recorded by ILSA showed a discontinuous pattern in the range − 20 °C to +60 °C. Fig. 5 shows the average temperature recorded by the sensors in the instrument during the entire period of its operation.

After initial 5 h of operation, the temperature started to decrease. This is attributed to the casting of shadow of the lander parts on the instrument. The built-in thermal control feature of ILSA was enabled during 16 to 48 h with a set value of 10 °C. The temperature was maintained within ±2 °C of the set value during this period.

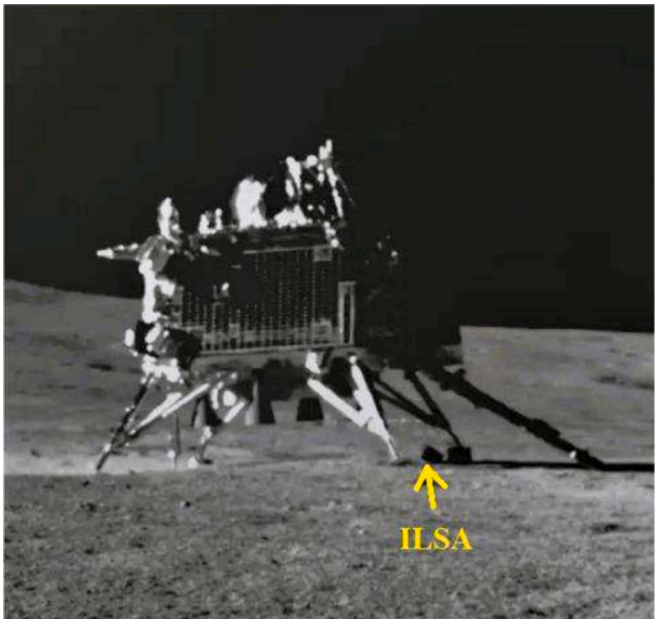

Fig. 4. ILSA deployed to lunar surface from the lander. The image is taken by the navigation camera of the Chandrayaan 3 rover.

Subsequently, the instrument was allowed to operate at the ambient temperature. After 70 h, the temperature started to increase as the instrument came out of the shadow. The value was stable within 50 °C to 60 °C during 110 to 170 h except for a period of six hours from 101 to 107 h. This is also attributed to the casting of shadow of any lander part on the instrument. The final dip and rise in temperature after 174 h of operation is due to stowing back and redeployment of ILSA. The dots at the top of the plot indicate the count of the 'uncorrelated events' recorded by the instrument and is discussed in Section 9. The lander had several temperature sensors on it distributed over various locations such as the top and bottom decks, the yaw and the pitch faces, the solar panels and the leg hinges. The sun elevation and azimuth angles as a function of time is obtained from the sun sensors on the lander. This information can be used to study the illumination and the shadowing on the instrument and is validated by the temperature records from various sensors. Very accurate modelling of the ambient temperature and the rate of heating and cooling at a given location demands more detailed analysis with additional input on the direct and indirect illumination as a function of time. The sensors in ILSA had a temperature dependence on their offset and the magnitude of the drift along each axis was obtained during the pre-flight ground calibration. The values are in the range of 20 to 100 $\mu g/^{O}C$. This is to be factored during the data analysis.

5. Data processing method

The output from ILSA was handled by the Bus Data Handling unit in the lander. Data was collected at a rate of 200 samples per second (sps) which is the sampling rate of fine range sensors. The data output rate of the coarse range sensors was 90 sps. At the instrument level, in the case of coarse range sensors, the value corresponding to the previous sample is repeated until the new data is updated. This must be considered while analysing the signals. The raw data in digital counts obtained from the sensors were converted to voltage and capacitance values for the fine range and coarse range sensors, respectively. This was then converted to acceleration in ms^{-2} using the conversion coefficients generated during the pre-flight ground calibration. This stage of data conversion is designated as Level 0 processing that generates output from the instrument in the form of 'comma separated values' (csv) files. The data after Level 0 processing is provided with UTC time stamping and is stored at the Indian Space Science Data Centre.

The data set from ILSA contains the following information (i) UTC Time stamping (ii) Coarse range sensor records along X, Y and Z axes (iii) Fine range sensor records along X, Y and Z axes and (iv) temperature information from all the three HMCs.

6. Preliminary observations

Our approach in the preliminary data analysis, definition of an 'event' and the methodology for identifying the nature of the events are discussed here.

The Level 0 data from ILSA is viewed using a standard plotting tool and is observed for variations in amplitude over time. When a noticeable variation in the amplitude is observed, the data in the given time frame is selected for further analysis. An *event* is defined when there is a distinguishable increase in the peak-to-peak amplitude in the recording for a certain duration of time and it symmetrically varies about its mean value. Most of the time, the output remained stable with a few bits of data toggling and there were several instances where it was stable even by one or two values over several seconds of duration. The instrument noise is practically obtained by estimating the power spectral density from the data recorded during the quiet hours with the ambient thermal conditions stable within 2 °C. Fig. 6 shows the instrument noise of the X axis sensor as a typical case.

When an event is observed from the recorded data, the following

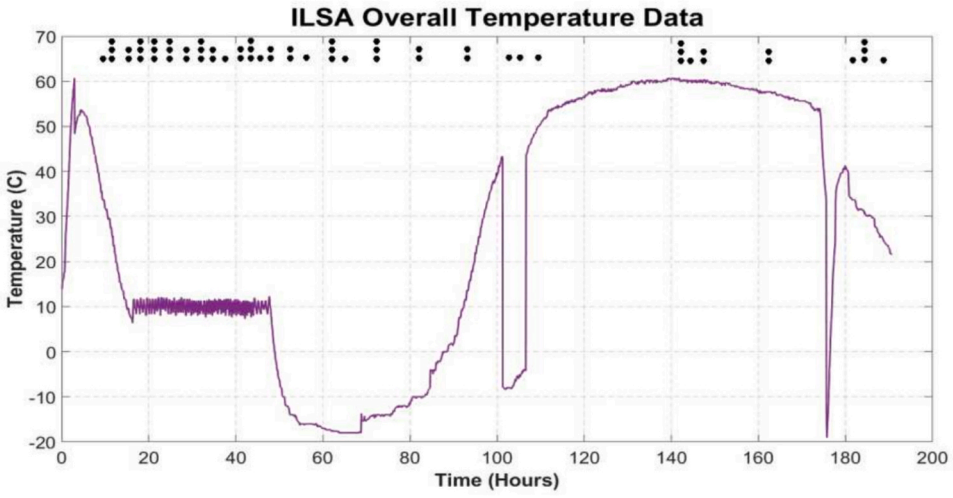

Fig. 5. Temperature experienced by ILSA during the entire operation period. The markers on the top shows the distribution of 'uncorrelated events'.

parameters associated with it are specifically studied:

(i) The amplitude of the signal
(ii) The time duration
(iii) The impulsive or emergent nature in the amplitude variation
(iv) Directionality of the signal by looking at the records on the other axes
(v) Frequency components in the signal

A summary of records is prepared based on the observations. Considering the basic definition of an event, we have catalogued about 250 distinct events with amplitudes in the range 1 μg to 5 mg and time duration varying from 1 s to 14 min. Events with lower amplitude and time duration are not counted in the present study. In most of the cases, signals are recorded simultaneously along all the three axes. In certain cases, there is difference in amplitude along different axes. The frequency components in the signals lie in the range 1 Hz to 60 Hz.

7. Event cataloguing and classifying approach

The catalogued events are distinguished by a unique identification number. This number encodes the UTC time at the beginning of the event in YYYYMMDDHHMMSS. From the first observation on the signals, we have handpicked about 200 records. Once a record is picked up, the next immediate step is to identify if it is caused by any known operational activity in the vicinity of the instrument that can cause ground vibrations. The event history from the mission provides this data. From this exercise, we could identify several activities that acted as sources of signals for ILSA as listed below:

(a) The navigation of the rover on the lunar surface.
(b) The operation of the Alpha Particle X Ray Spectrometer (APXS) payload on the rover that has a mechanism involving physical movement of its parts.
(c) The insertion of a probe of the ChaSTE payload on the lander into the lunar regolith by motorized movement.
(d) The deployment of the Langmuir Probe (LP) on the lander which was a one-time operation after landing.

The records of ILSA generated by these known activities are designated as “correlated events”. The event identification number will carry a suffix C for these kinds of records.

There are about 50 records whose cause could not be correlated to any known operation in the lander or rover. Such records are classified as “uncorrelated events”. The event identification number are given a suffix U in these cases. Uncorrelated events are of special interest and the cause of such events are to be studied carefully.

8. A preliminary analysis of ‘correlated events’

8.1. Rover navigation

The longest and relatively large amplitude records from ILSA are those corresponding to the navigation of the rover on the lunar terrain. The longest continuous signal record lasts for 14 min. About 60 signals catalogued correspond to the rover movement which is controlled by ground commands. The rover that weighed about 25 kg had six wheels and was driven with motors. It moved at a typical speed of 1 cm per second. The dynamics of the rover and the wheel-soil interaction had been a source of complex ground vibration signal input to ILSA. As the distance of the rover from ILSA was increased, there had been a systematic reduction in the amplitude of the signal under normal roving conditions. For example, when the rover was away from the lander by around 7 m, the average peak to peak amplitude was around 200 μg. This amplitude was halved when the distance became 12 m and was one order less when the separation was 40 m. Figs. 7 and 8 show the records by ILSA during the navigation and manoeuvring operations of the rover at two occasions on 25 August 2023 and 27 August 2023, respectively. The record in Fig. 7 corresponds to a travel of about 5 m and two manoeuvring operations to turn the rover by 12^{O} in clockwise (CW) and counter clockwise (CCW) directions. The CW turning was commanded after a translation of 2.8 m and the CCW turn was at the end. Fig. 8 is the record during a 30^{O} CCW turning operation. There were multiple

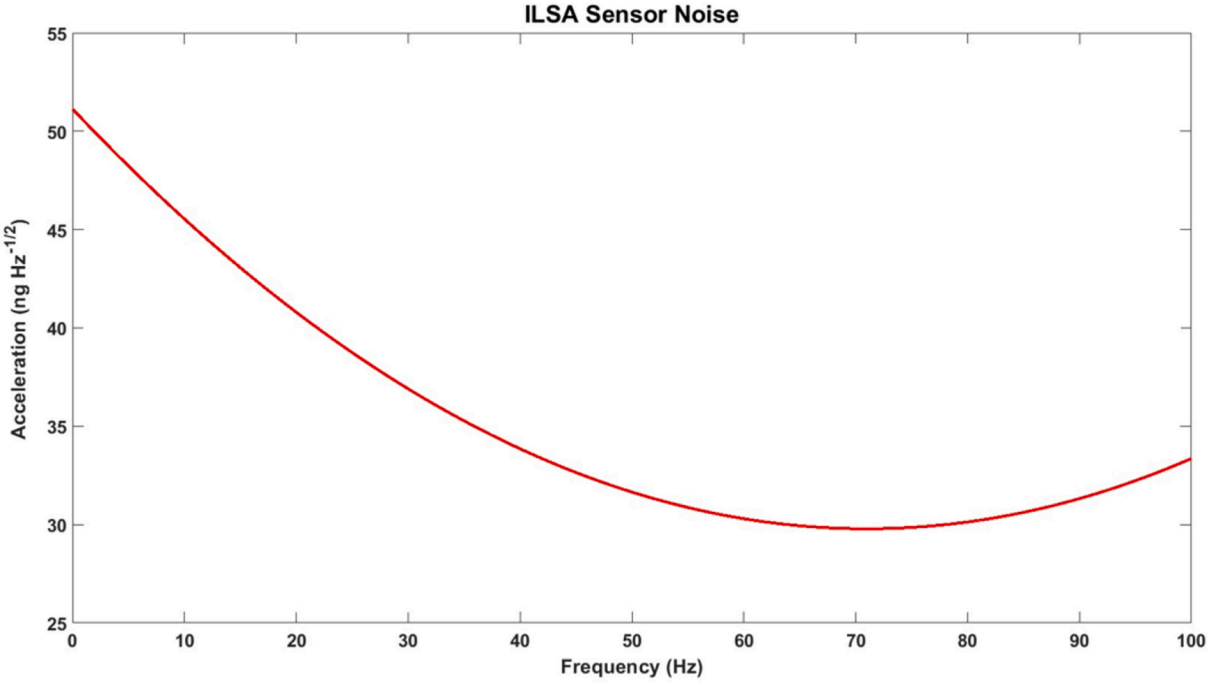

Fig. 6. The instrument noise. The plot shows the acceleration noise spectral density generated from the output of X axis sensor during quiet period of operation at Moon.

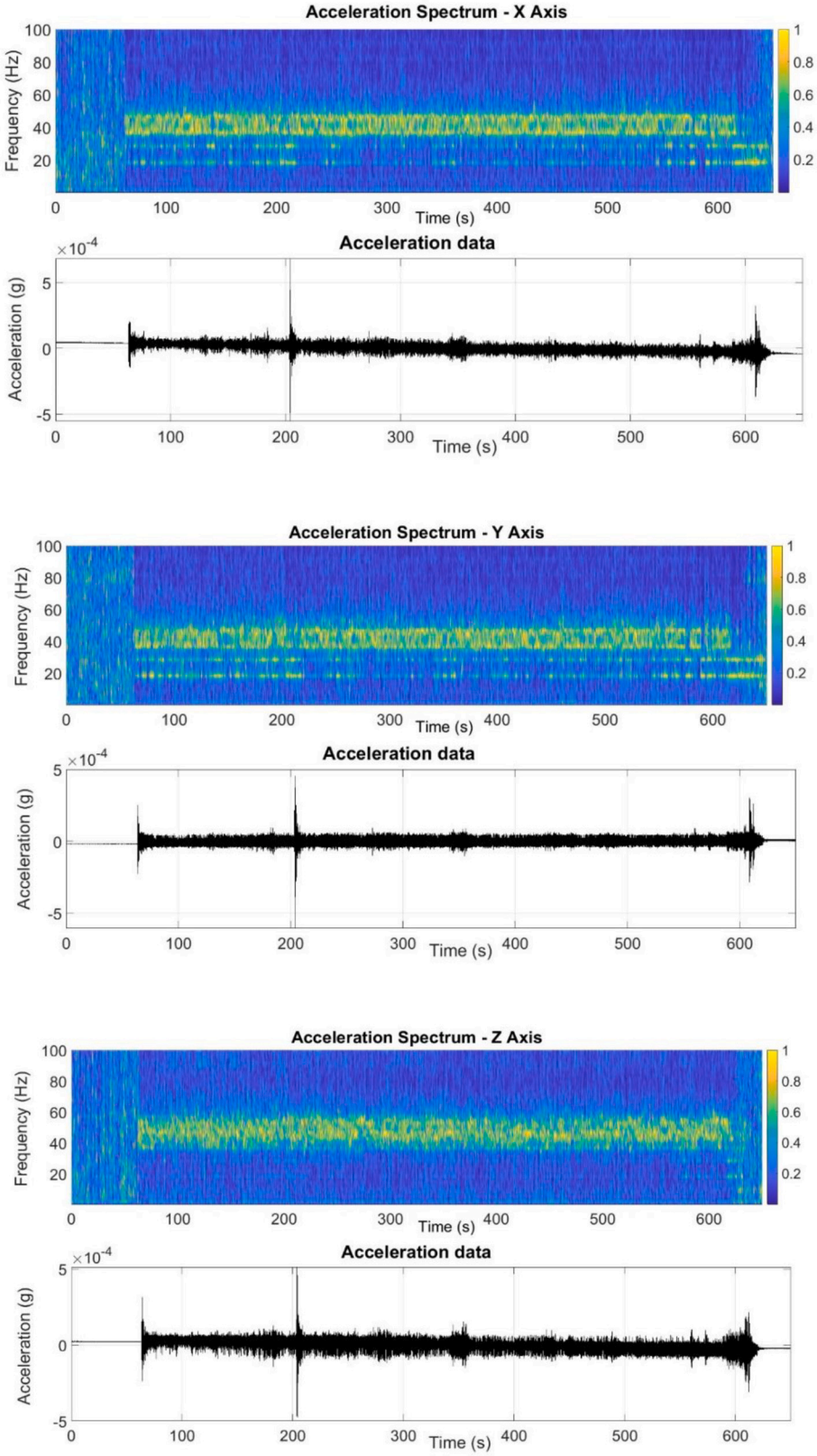

Fig. 7. Response of ILSA to rover navigation on lunar terrain on 25 August 2023 (Event Id - 20230825185842C). The acceleration data along X, Y and Z axes and the corresponding spectrograms are shown. The spectrograms are generated from the FFT of the unfiltered, baseline-corrected data for a window size of 0.5 s. The output is smoothened and normalised in each window.

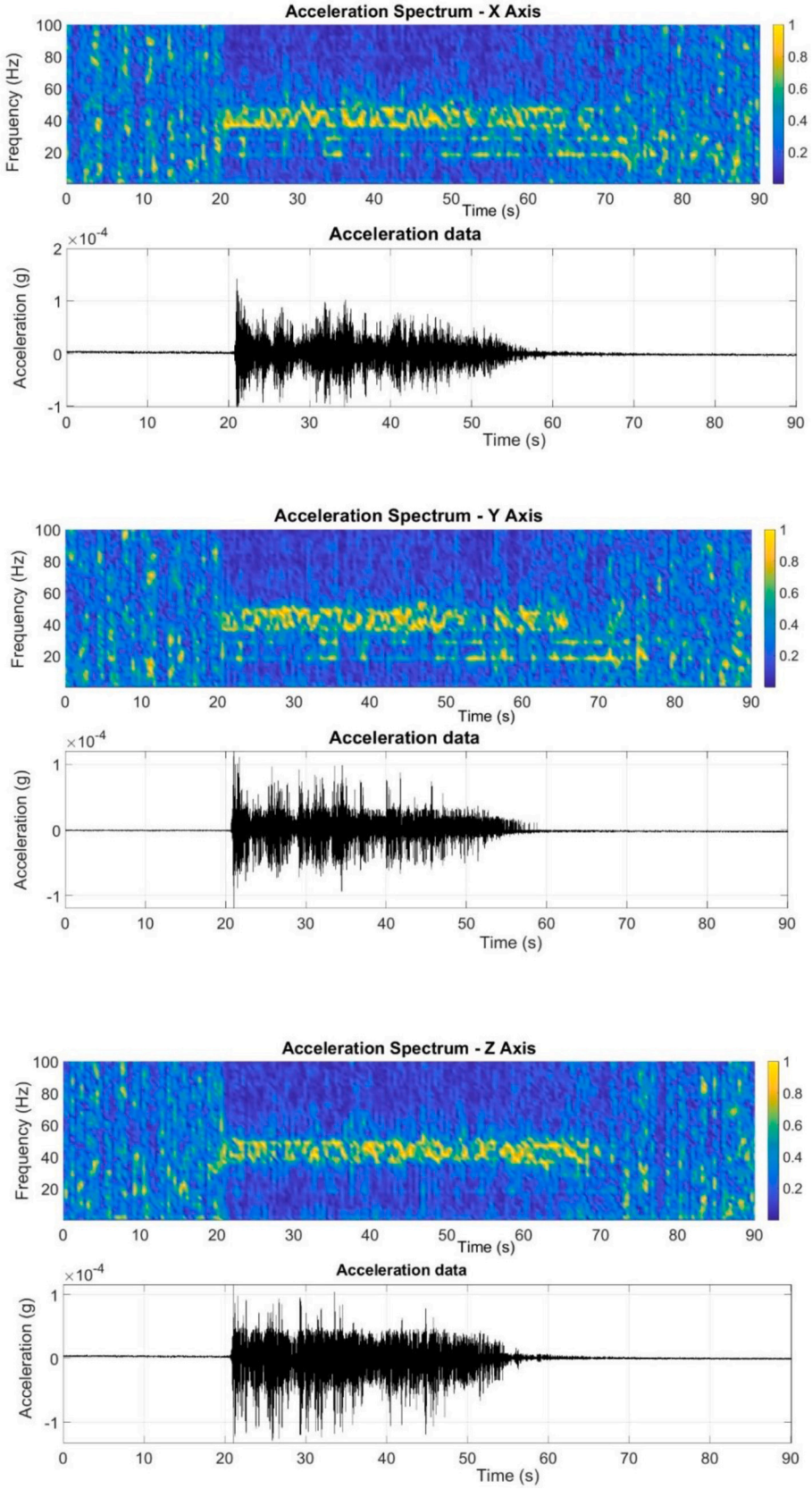

Fig. 8. Response of ILSA to rover manoeuvring operation on lunar terrain on 27 August 2023 (Event Id 20230827160331C) showing the acceleration data along X, Y and Z axes and the corresponding spectrograms. For further explanation, see Fig. 7.

instances of manoeuvring the rover for its orientation change and these commands were sent as a part of hazard avoidance. The details of rover navigation steps will be separately indicated along with the data when released for analysis. The plots show the acceleration amplitude in 'g' and the corresponding spectrogram. The spectrogram is generated from the Fast Fourier Transform (FFT) of the data for a window size of 0.5 s. The output is smoothened and normalised with respect to maximum spectral amplitude in each window. The acceleration data is unfiltered, but applied with baseline correction and Tukey windowing with $r = 5$ % before taking the FFT. The plots presented are in the linear scale. This approach is adopted for all spectrograms presented in this paper. The distinct increase in the amplitude of the signal corresponds to the onset of the rover movement. Certain random peaks in the signal could be attributed to local effects in the wheel interactions with the soil that contains pebbles and stones distributed over the regolith. The amplitudes of the signals are in the range of 100 to 300 μg. The total duration of signal in this case is around 550 s. X and Y sensors have major frequency components at 40 and 23 Hz, whereas the Z sensor has dominant energy in 47 to 59 Hz range. In all cases, lower frequency components at around 4 Hz are also present. A systematic study on the signals at various distances and orientations of the rover with respect to ILSA will be carried out separately in future. The frequency components of 23 Hz and 40 Hz are attributed to the eigen modes associated with the rover structure and the subsystems in it. The global lateral mode of vibration of the lander is around 5 Hz. An idea about the vibrational modes associated with the lander and the rover is obtained by structural modelling and analysis. Vibration modes of the main structure and selected subsystems are recorded during the pre-flight vibration tests and this data is used to validate the simulation results.

8.2. APXS payload operation

Another source of signal for ILSA was the operation of APXS payload on the rover. The primary objective of the payload was to determine the elemental composition of lunar surface in the surrounding regions of the landing site. This is achieved by X-ray fluorescence spectroscopy technique. An in situ radioactive excitation source emitting X-ray and alpha particles and the detectors were the two important building blocks of the instrument. APXS was mounted on the bottom chassis of the rover. During the operation of the instrument the rover was not moving. A deployment mechanism was used to bring the source and detectors close to the lunar surface for carrying out the measurements and stow it back after the completion (Shanmugam et al., 2020). Operation of a brushless DC (BLDC) electric motor and the latching at microswitches associated with the mechanism were the sources of mechanical signals transmitted to ILSA through the lunar soil. Each operation of the payload caused a unique recording by ILSA. The response of ILSA to APXS mechanism operation on 29 August 2023 along with the spectrogram is shown in Fig. 9. The separation between the instruments was around 7 m at this time. A typical record in this case lasts for around 40 s. The peak amplitude of the signal is around 300 μg. The dominant frequency components in the signal lies at 23 and 25 Hz along all axes. Some energy is also found near 37 Hz for the Z axis sensor. The frequency components observed during APXS operation could be attributed to the modes excited in the rover and its subsystems.

8.3. ChaSTE payload operation

The ChaSTE payload in the lander aimed to study the thermal properties of the lunar regolith at the landing site by in situ measurement of vertical temperature from the surface. The payload is a thermal probe carrying ten Platinum Resistance Thermometers in it distributed over the sensing region. After the deployment of the probe from the lander, it was inserted into the lunar regolith in a controlled manner using a BLDC motor and ball-screw based mechanism. The overall depth of penetration of the probe into lunar regolith was around 145 mm. ILSA and ChaSTE were separated by about 1 m. The records by ILSA during the ChaSTE operation on 25 August 2023 is given in Fig. 10 and that on 3 September 2023 is given in Fig. 11. The depths of penetration of the probe were approximately 140 mm and 107 mm, respectively. The amplitude of the signal is around ten times higher in this case compared to the response to rover and APXS operations. As the drilling advanced deeper into the lunar soil, the amplitude of the signal recorded by ILSA systematically increased. The recorded data shows the presence of several high frequency components. The global lateral and longitudinal modes of the lander structure have values around 5 Hz and 10 Hz. The frequencies of subsystem elements associated with lander such as the solar panels, the liquid engine assemblies and the leg assemblies have values above 30 Hz. The presence of high frequency components in the data during ChaSTE operation may be due to the excitation of lander subsystems during the probe insertion process. The amplitudes of the high frequency components are found to be larger in the post hop data. The presence of 2 Hz component observed in the signals recorded on 25 August 2023 data may be attributed to the excitation of the LP probe-boom system which was in a deployed state. This component was observed after the deployment of the probe as well. However, this is not observed in the post hop records. This needs further analysis and careful investigation combining with the operational details of the probe. The absence of 23 Hz component, which is assumed to be the rover mode, in the post hop on data could be due to the larger distance of separation between the rover and the lander compared to that on 25 August 2023.

8.4. Langmuir probe deployment

The Langmuir Probe was the part of the payload having the objective of measuring near surface plasma environment at the landing site (Manju et al., 2020). The probe was fixed at the free end of a boom that was attached to the top deck of the lander. A hold down and release mechanism was used to deploy the boom. The LP-boom system was deployed on 24 August 2023 and was a one-time operation. The deployment was carried out before the offset correction of the fine range sensors of ILSA. Hence signals corresponding to this operation were recorded only by the coarse range sensors. The data from z-axis coarse sensor is reported in this specific case and is shown in Fig. 12. The amplitudes are smaller by an order of magnitude in the X and Y sensors. The dominant frequency components in the signal are below 5 Hz in this case. This could be interpreted as the excitation of the lander modes and the post deployment vibration of the probe-boom system itself.

9. A preliminary analysis of 'uncorrelated events'

From the data investigated as a part of this paper, there are about 50 instances where the amplitude of output from the instrument is distinguishably different from its normal background level. From the mission command history, it was confirmed that any activity that can cause ground vibration was not performed during this timeframe. Hence these are identified as 'uncorrelated events'. The maximum peak to peak amplitude of the signal is as high as 700 μg in certain instances. The frequency content in the signals are spread over a wide range up to 50 Hz. The signals discussed here lasted only for a few seconds. Although several distinct signals lasting less than a couple of seconds are also observed, they are not included in the count reported in this paper.

Any event that could be classified as deep quake or shallow quake was beyond the targeted objectives and design specifications of ILSA. We were aware of the very low probability of occurrence of those classes of events during the one lunar day operation of the instrument. All the uncorrelated signals recorded by ILSA have high frequency components in it. Short duration seismic signals containing high frequency energy were recorded by short period seismometers and geophones in the Apollo missions (Duennebier and Sutton, 1974a; Civilini et al., 2023; Duennebier and Sutton, 1974b). High frequency signals including a class of super high frequency events were recorded on the Mars by the InSight

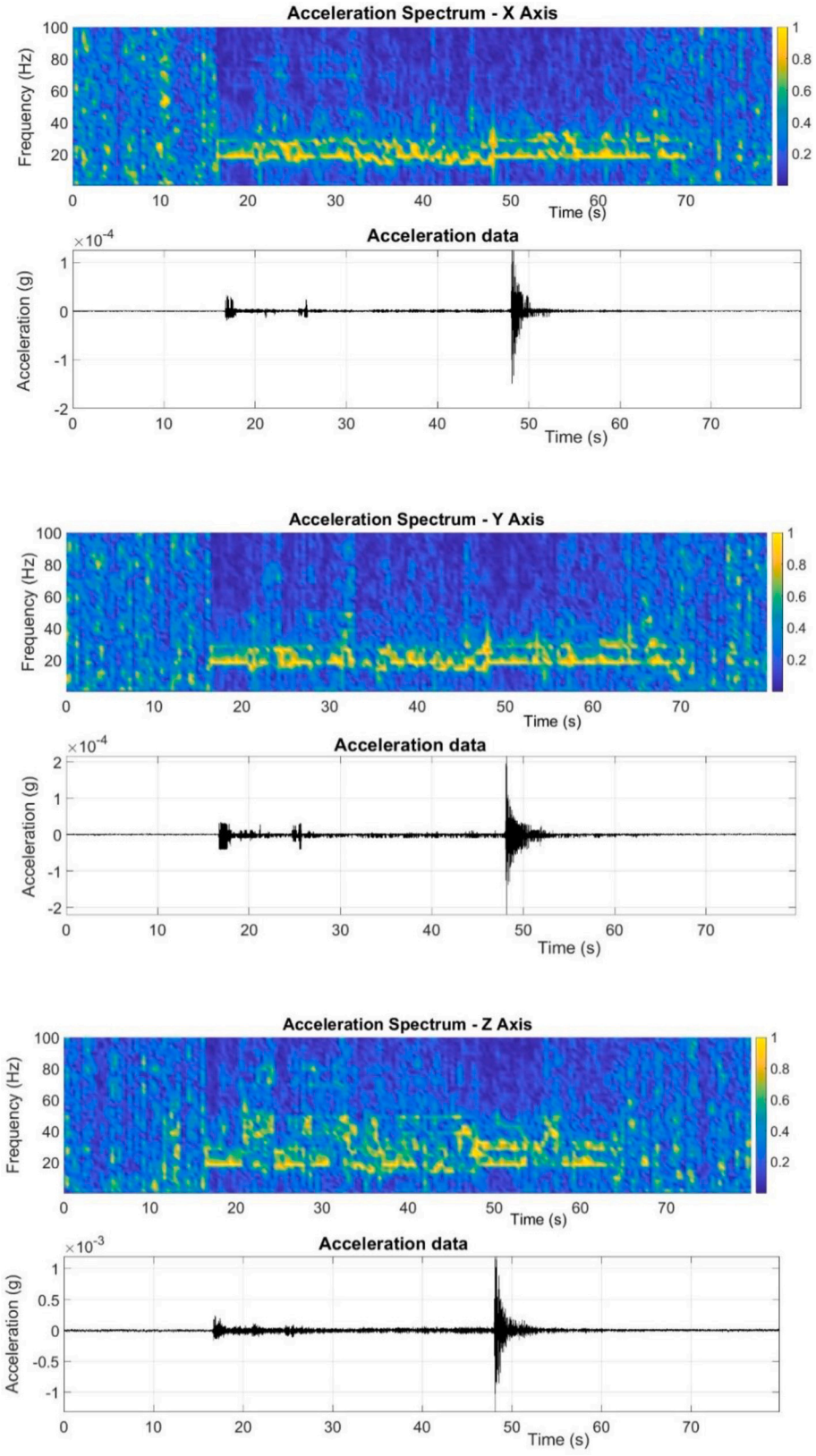

Fig. 9. Response of ILSA to APXS payload operation on 29 August 2023 (Event Id - 20230829193657C) showing the acceleration data along X, Y and Z axes and the corresponding spectrograms. For further explanation, see Fig. 7.

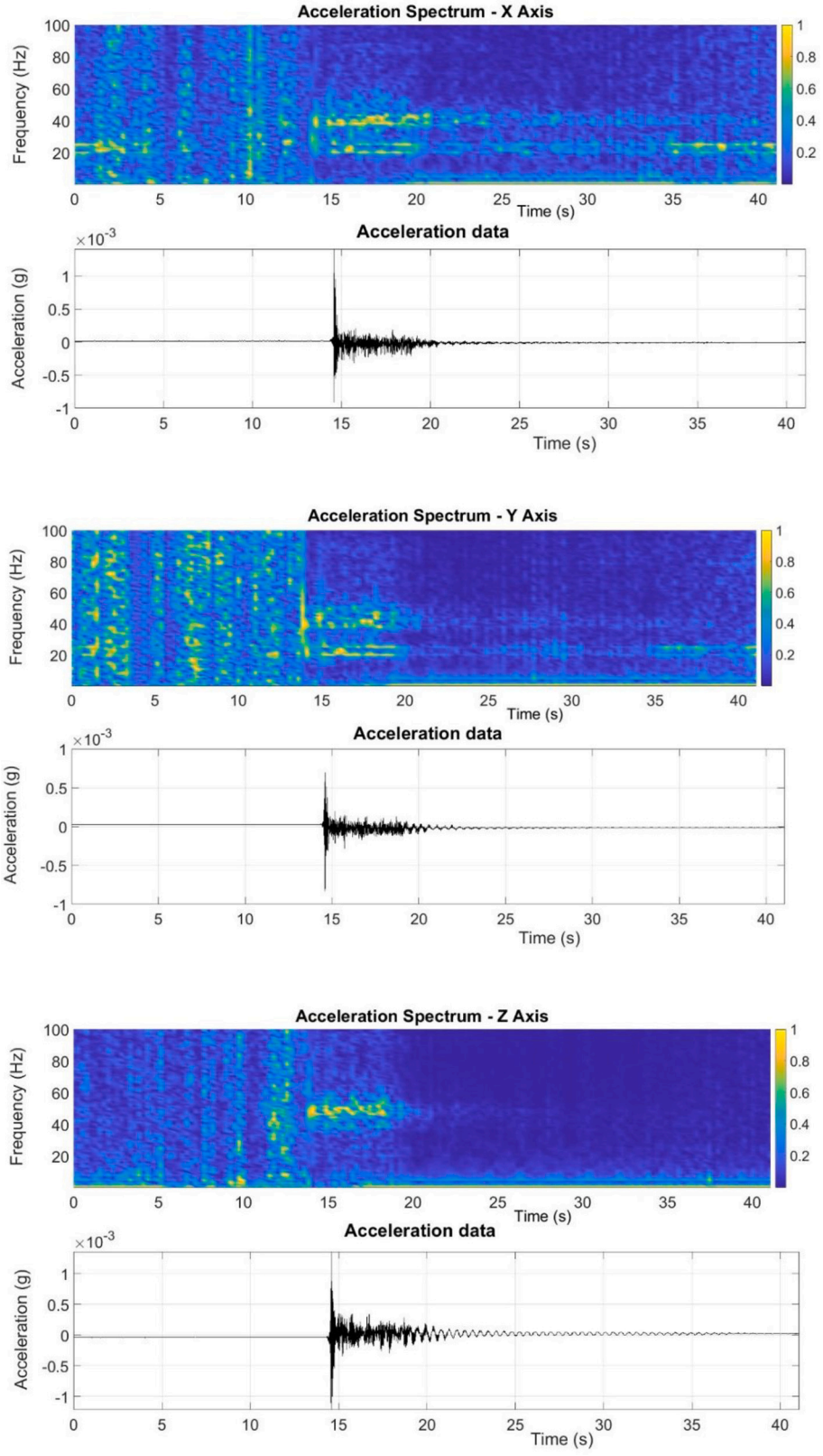

Fig. 10. Response of ILSA to ChaSTE payload probe operation on 25 August 2023 (Event Id - 20230825153514C) showing the acceleration data along X, Y and Z axes and the corresponding spectrograms. For further explanation, see Fig. 7.

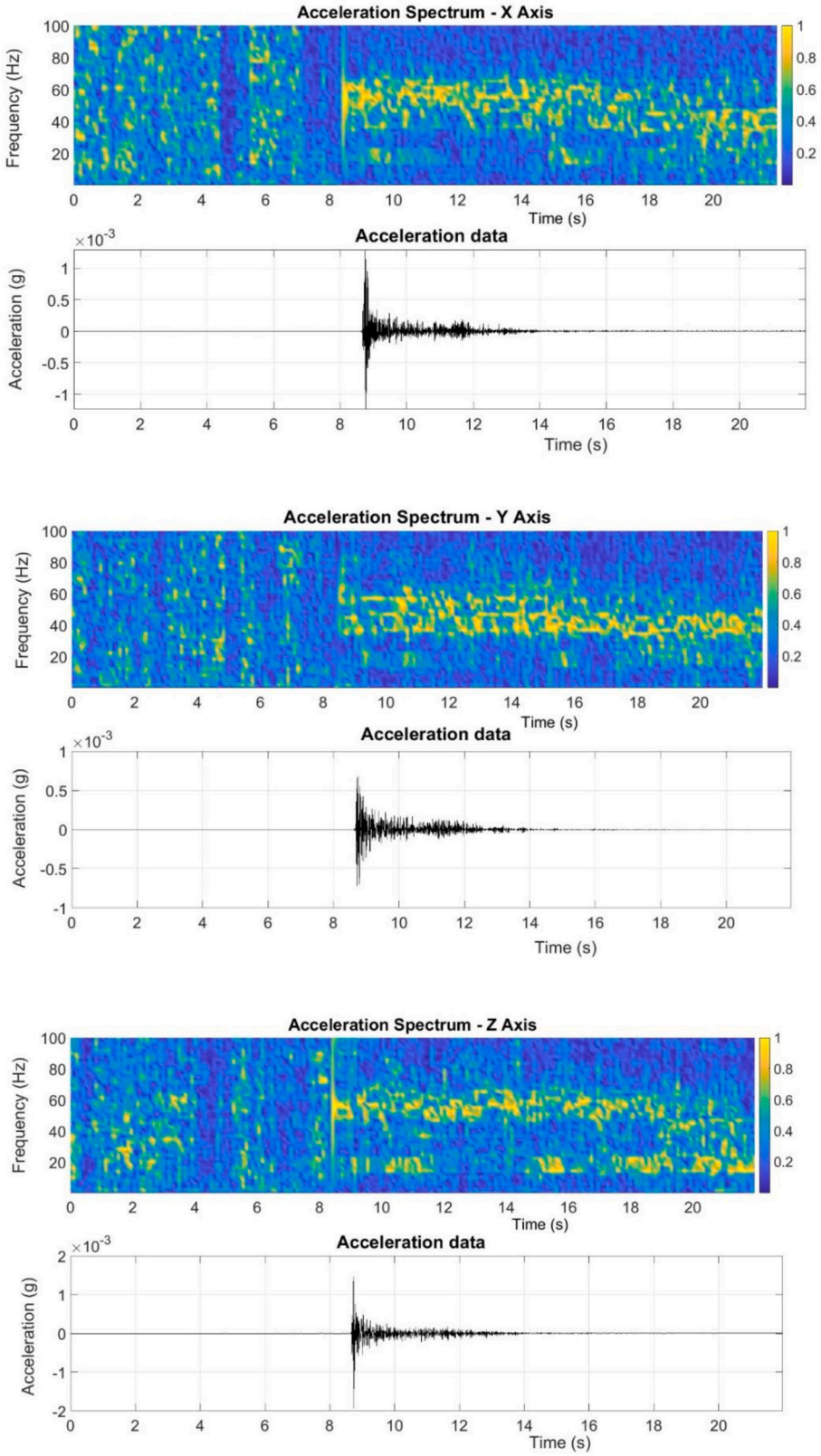

Fig. 11. Response of ILSA to ChaSTE payload probe operation on 3 September 2023 (Event Id - 20230903001825C). The lander is at new location 50 cm away compared to that in Fig. 10. The acceleration data along X, Y and Z axes and the corresponding spectrograms are shown. For further explanation, see Fig. 7.

seismometers (Nikolaj et al., 2021). All these instruments have recorded data at different sampling rates. The 'uncorrelated event' records of ILSA are observed to have following signatures: (i) impulsive onsets (ii) intermediate or emergent onsets. This classification of signals is based on the rise time to reach maximum amplitude of the signal energy and is based on the approach reported in (Dimech et al., 2024). Signals of these types are observed in the Moon and the Mars data (Civilini et al., 2023; Duennebier and Sutton, 1974b).

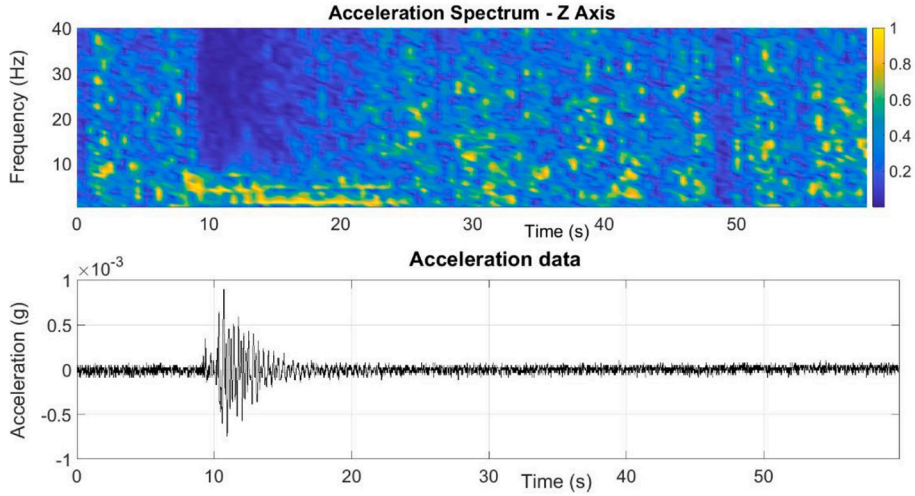

Fig. 12. Response of *Z*-axis coarse range sensor of ILSA during the deployment of the Langmuir Probe located on the Lander on 24 August 2023 (Event Id - 20230824115937C). The acceleration data and the corresponding spectrogram is shown. For further explanation, see Fig. 7.

Chandrayaan 3 landed on the Moon after the beginning of a lunar day which is approximately equal to fourteen Earth days. The face of the lander opposite to the rover ramp, designated as +Yaw, was illuminated during the entire mission duration. Two adjacent faces, +Pitch and -Pitch were partially illuminated and the amount of solar flux was slowly varying over time. -Yaw face where rover ramp is present was not directly illuminated. This is evident from the photograph given in Fig. 4. Temperature profiles obtained from various sensors in the lander indicate that there were no transitions in temperatures beyond 3 °C per hour at most of the structural elements. ILSA started its operation 48 h after the sunrise and was powered off at least 24 h before the sunset. The probability of thermal relaxation of the lander structure triggered by sudden transitions in temperature and thereby causing ground vibrations is assumed to be low. Any mechanical excitation of the structural elements triggered by leakage of fuel through the pipes or venting through the valves is also not suspected. This information is obtained by referring to the data recorded by various sensors integrated to the propulsion system. By design and detailed structural analysis of the ILSA, there are no parts that can be source of vibrations below 80 Hz.

The short period seismometers in Apollo stations have reported magnetically induced signals with high frequency content lasting for a few seconds. The reason attributed to those observations is inductive coupling of rapid changes in the lunar magnetic field with the coil of the seismometers (Duennebier and Sutton, 1974a). Since ILSA employs silicon based open loop capacitive sensor and does not use any magnetic material in its construction, this possibility can be ruled out as a cause of uncorrelated signals. The uncorrelated signals recorded by ILSA may be due to: (a) impact of micrometeorites at near ranges of the instrument (b) local thermal effects on the soil (c) thermal adjustments within the lander subsystems. Signals generated by the impact of micrometeorites and local thermal effects are recorded by Apollo short period instruments (Latham et al., 1973). Events with significant high frequency energy content could be due to meteoroid impacts as reported in (Duennebier and Sutton, 1974b). The spectrogram for the impacts shows the presence of energy up to 15 Hz. However, the possibility for presence of energy at higher frequencies is not discussed in this paper. Thermal moonquakes generated by natural processes occurring on the lunar surfaces is reported in (Duennebier and Sutton, 1974a). These signals are also characterised by the presence of high frequency components in it. The local shadowing and illumination of the surface and the resultant temperature variations can cause thermal stresses and relaxations in the lunar materials. It is to be noted that the lunar soil near the instrument was disturbed by the navigation and manoeuvring of the rover. Another possible source of uncorrelated signals would be the thermal adjustments of structural elements associated with the lander and the rover subsystems. Due to variation in sun illumination angle, there would be shadowing effect on certain parts leading to local fluctuations in temperature. The energy associated with the thermal relaxations could be transmitted to ILSA through the lunar regolith. Fig. 5 shows that ILSA experienced a large temperature variation during its period of operation. This includes a rapid transition of around 10 °C/min at 101 and 107 h after the power on. However, the distribution of uncorrelated events is nearly uniform over the entire period of operation. There is no clustering of signals during the time period of sudden transition of temperature of the instrument. Hence the possibility of thermal relaxation of the instrument itself as a source of signal can be ruled out. It will be interesting to study some of the signals from ILSA referring to the super high frequency events recorded by InSight Seismometer on Mars as discussed in (Nikolaj et al., 2021). Methods are to be developed to identify the uncorrelated signals that could have originated from the lander or the rover as 'donks' and 'glitches' discussed in this paper. There are also certain signal records with specific patterns that needs further understanding. The potential sources of the signals recorded by ILSA reported in this section requires detailed studies and investigations.

Figs. 13–15 summarizes the various types of records classified as uncorrelated events obtained by ILSA. Fig. 13 shows a typical event recorded on 26 August 2023 with a longer rise time compared to that that shown in Fig. 14. In this case the vertical component has a lower amplitude compared to the horizontal components. In the record corresponding to Fig. 14 recorded on 27 August 2023 the signal is more 'impulsive' in nature and the vertical component is slightly stronger than the horizontal components in the peak to peak amplitude. A unique record obtained on 1 September 2023 that could not be correlated to any commanded activity of the lander or the rover is given in Fig. 15. This data has unusually very high frequency components compared to other signals.

The summary of observations and distinct features of selected signals presented in this paper is given in Table 1. The frequency content mentioned in the Table are in the order of high to low amplitude and those signals with less than around 25 % of highest amplitude are not included.

10. Conclusion

This paper summarizes the overall operation of ILSA on Moon presenting the preliminary data. The instrument demonstrated the successful usage of silicon MEMS devices in lunar environment along with its capability to survive the various operation phases including the

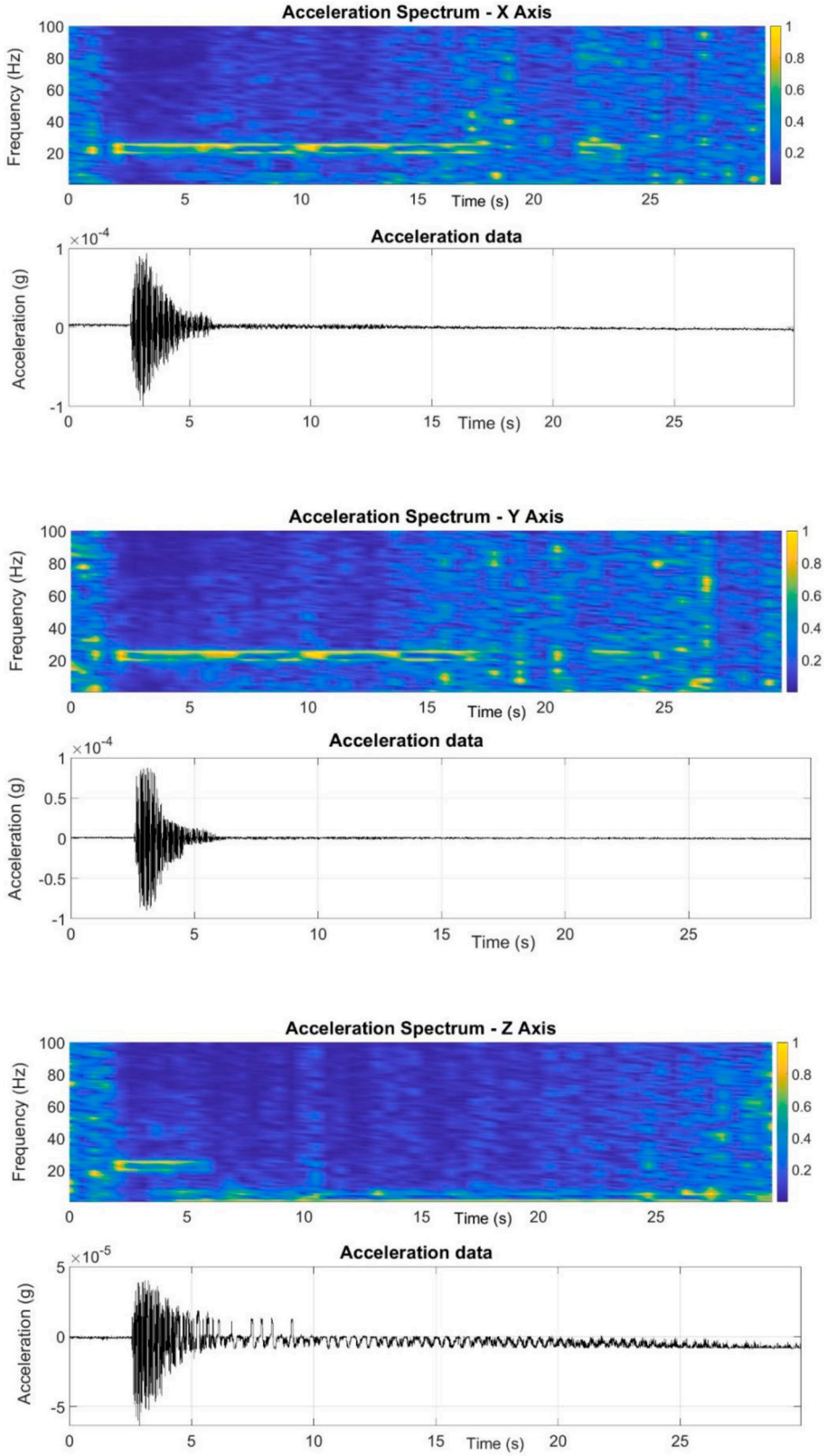

Fig. 13. Event with emergent/intermediate onset recorded by ILSA on 26 August 2023 (Event Id - 20,230,826,212,117 U). The acceleration data along X, Y and Z axes and the corresponding spectrograms are shown. For further explanation, see Fig. 7.

landing. The data from ILSA is the first ever seismic signal recorded from an instrument deployed at the lunar polar region. An approach is developed for assigning event identification number and for classifying them based on its source. The amplitude plots and the corresponding spectrogram for selected events are given. Also, a preliminary understanding of correlated and uncorrelated events is briefly discussed. Even though the possible causes of signals due to uncorrelated events are presented, detailed analysis has to be conducted to get more insights

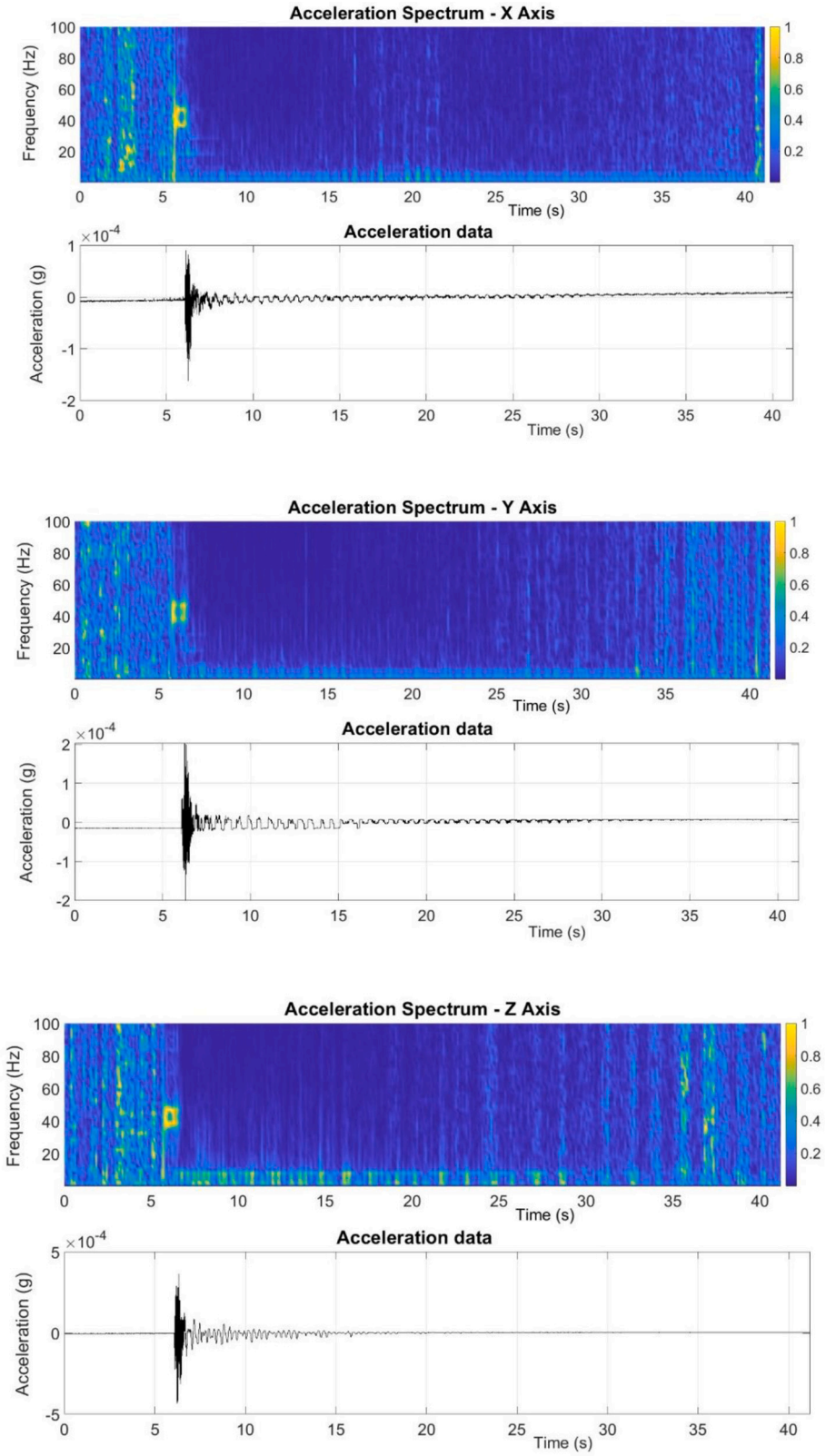

Fig. 14. Event with 'impulsive' onset recorded on 27 August 2023 (Event Id 20,230,827,003,355 U). The acceleration data along X, Y and Z axes and the corresponding spectrograms are shown. For further explanation, see Fig. 7.

from the records.

CRediT authorship contribution statement

J. John: Project administration, Investigation, Conceptualization. **V. Thamarai:** Writing – review & editing. **Teena Choudhary:** Formal

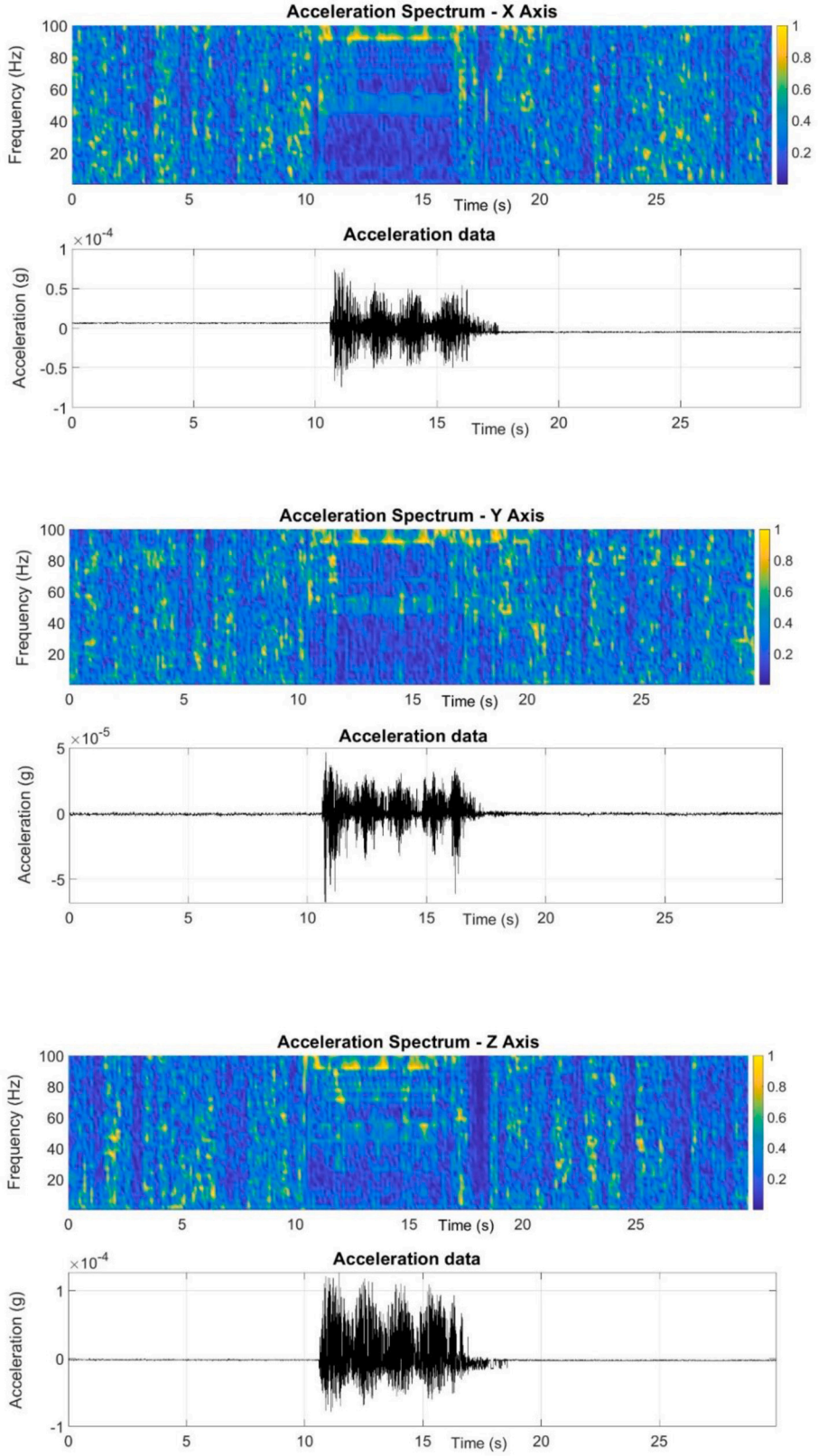

Fig. 15. Uncorrelated event with very high frequency content recorded on 1 September 2023 (Event Id 20,230,901,065,715 U). The acceleration data along X, Y and Z axes and the corresponding spectrograms are shown. For further explanation, see Fig. 7.

Table 1
Key features in 9 selected records of ILSA.

Event Id	Event	Key features of the signals
20230825185842C	Rover navigation, 25 August 2023	Duration (s): 550 Frequency content (Hz): X and Y axes: 40, 23 and 4, 34 Z axis: 47–50, 40, 23 and 4, 34
20230827160331C	Rover manoeuvring, 27 August 2023	Duration (s): 35 Frequency content (Hz): X axis: 40, 23 and 4 Y axis: 43, 40, 23, 4 Z axis: 43, 40, 23
20230829193657C	APXS payload operation, 29 August 2023	Duration (s): 40 Frequency content (Hz): X axis: 23, 28 Y axis: 23, 28, 30, 37 Z axis: 23, 37, 29, 36
20230825153514C	ChaSTE payload operation, 25 August 2023	Duration (s): 10 Frequency content (Hz): X axis: 22, 37, 39–41, 2 Y axis: 23, 39, 2,37 Z axis: 2, 46, 49, 40, 37
20230903001825C	ChaSTE payload operation, 3 September 2023	Duration (s): 8 Frequency content (Hz): X axis: 55, 58, 51,18, 39, 41 Y axis: 40, 39, 51, 18 Z axis: 18, 58, 53, 51, 40, 43
20230824115937C	LP deployment, 24 August 2023	Duration (s): 15 Frequency content (Hz): Z axis: 5, 3, 2
20230826212117U	Uncorrelated, 26 August 2023	Duration (s): 5, longer along z direction Frequency content (Hz): X axis: 23, 15 Y axis: 23, 15 Z axis: 23, 2, 5, 4, 15
20230827003355U	Uncorrelated, 27 August 2023	Duration (s): 10, longer along x and y directions Frequency content (Hz): X axis: 2, 41, 22 X axis: 2, 41, 4, 6, 22 Y axis: 4, 6, 41,2
20230901065715U	Uncorrelated, 1 September 2023	Duration (s): 8, longer along x and y directions Frequency content (Hz): X axis: 94, 49 Y axis: 94, 49, 76, 50, 60 Z axis: 94, 80, 74, 49

analysis, Data curation. **M.N. Srinivasa:** Formal analysis, Data curation. **Ashwini Jambhalikar:** Methodology. **M.S. Giridhar:** Writing – review & editing. **Madan Mohan Mehra:** Writing – review & editing. **Mayank Garg:** Data curation. **K.V. Shila:** Methodology. **Krishna Kummari:** Formal analysis, Data curation. **S.P. Karantha:** Writing – review & editing. **Kalpana Arvind:** Writing – review & editing, Supervision. **K.V. Sriram:** Supervision.

Declaration of competing interest

The authors declare that they have no known competing financial interests or personal relationships that could have appeared to influence the work reported in this paper.

Data availability

The data discussed in the paper will be released through Indian Space Science Data Centre in future once the Organisation gives clearance for the same.

Acknowledgement

The authors are extremely thankful to ISRO for selecting ILSA payload for Chandrayaan mission and funding the project. We are grateful to Shri S Somnath, Chairman, ISRO and Shri M Sankaran, Director, U R Rao Satellite Centre (URSC) for their overwhelming support. A big thanks to the team of engineers and technicians of LEOS and URSC who were a part of building, testing, qualifying ILSA and integrating it to the spacecraft. We are indebted to distinguished scientists, Dr. T K Alex and Dr. A S Kirankumar for closely following up the development of the instrument and reviewing its performance at various stages of its realization and on orbit operations. Our heartfelt thanks to Dr. D Srinagesh, and his team at CSIR-NGRI for the invaluable and continual support right from the conception of the idea to have this instrument on the Moon. We thank Dr. Anil Bhardwaj and all other scientists who reviewed the instrument and the data recorded by it. Our heartfelt thanks are due to Shri J A Kamalakar, Shri Laxmiprasad, Dr. G N Rao, Shri Elumalai and Dr. Rafiqul Islam for their guidance during the evolution of the instrument. The authors would like to specifically thank the Chandrayaan 3 Project Director and the entire team along with the Mission and Data handling teams for their crucial roles in placing and operating ILSA and handling the data. We thank the Mechanisms team of URSC for deploying the instrument safely to the lunar surface. We also grateful to the Thermal, Structures and Propulsion teams for sharing the information required for the understanding of the data. We thank Shri Prabakaran and team of URSC for processing the Level 0 data and making the quick look display see it on a monitor. We are very grateful to Shri Himanshu Pandey, Shri Sreenatha R and their team at ISRO Telemetry, Tracking and Command Network for facilitating the availability of data. Thanks to Pratheek T K, Akshay, Raju, Trupti and Rajendra at LEOS for their meticulous work in calibrating the instrument and consolidating the data. We record our sincere gratitude to the fellow science instrument teams and the rover team who shared information on the operation of the payloads. We acknowledge the support from KHMD Ltd. Bangalore for developing the hybrid package and Central Power Research Institute, Bangalore for supporting the characterisation of the instrument.

References

Amitabh, Suresh, K., et al., 2023. Terrain characterisation of potential landing sites for Chandrayaan-3 lander using orbiter high resolution camera (OHRC) images. In: 54th Lunar and Planetary Science Conference (LPI Contrib. No. 2806).

Civilini, F., Weber, R., Husker, A., 2023. Thermal moonquake characterization and cataloging using frequency based algorithms and stochastic gradient descent. JGR Planets. https://doi.org/10.1029/2022JE007704.

Dimech, J.L., et al., 2024. Preliminary analysis of newly recovered Apollo 17 seismic data. In: Results in Physics. Elsevier. https://doi.org/10.1016/jrinp.2017.11.029.

Duennebier, Frederick, Sutton, George H., 1974a. Thermal moonquakes. J. Geophys. Res. 79 (29).

Duennebier, Frederick, Sutton, George H., 1974b. Meteoroid impacts recorded by the short-period component of Apollo 14 lunar passive Seismic Station. J. Geophys. Res. 79 (29).

Durga Prasad, K., Bhatt, Megha, et al., 2023. Contextual characterization study of Chandrayaan-3 primary landing site. MNRAS 526, L116–L123. https://doi.org/10.1093/mnrasl/slad106.

Gary, V., Latham, Ewing, Maurice, et al., 2024. Passive seismic experiment. Science 167 (3918). https://doi.org/10.1126/science.167.3918.455.

Harms, Jan, 2022. seismic background limitation of lunar gravitational wave detectors. Phys. Rev. Lett. 129, 071102 https://doi.org/10.1103/Physrevlett.129.071102.

John, J., et al., 2020. Instrument for lunar seismic activity studies on Chandrayaan-2 Lander. Curr. Sci. 118 (3), 10.

John, F., Clinton, et al., 2021. The marsquake catalogue from insight sols 0–478. Phys. Earth Planet. Inter. 310, 106595 https://doi.org/10.1016/jpepi.2020.106595.

Knapmeyer-Endrun, Brigitte, Kawamura, Taichi, 2020. NASA's InSight mission on Mars-first glimpses of planet's interior from seismology. Nat. Commun. 11, 1451. https://doi.org/10.1038/s41467-020-15251-7.

Latham, G., Dorman, J., et al., 1973. Moonquakes, meteoroids, and the state of the lunar interior. In: Proceedings of the Fourth Lunar Science Conference, (Supplement 4, Geochimica et Cosmochimica Acta), 3, pp. 2515–2527.

Lognonne, P., et al., 2019. SEIS: InSight's seismic experiment for internal structure of Mars. Space Sci. Rev. 215, 12. https://doi.org/10.1007/S11214-018-0574-6.

Lognonne, P., Johnson, C.L., 2015. Planetary seismology. In: Treatise in Geophysics, , Second edition10, pp. 65–120. https://doi.org/10.1016/B978-0-444-53802-4.00167-6.
Lorenz, R.D., Nakamura, Y., 2013. Viking seismometer record: data restoration and dust devil search. In: 44th Lunar and Planetary Science Conference, p. 1178.
Manju, G., Pant, Tarun K., et al., 2020. Lunar near surface plasma environment from Chandrayaan-2 Lander platform: RAMBHA -LP payload. Curr. Sci. 118 (3).
Nakamura, Yosio, 1978. Moonquakes: source distribution and mechanism. In: Proc. Lunar Planet Sci Conf 9th, pp. 3589–3607.
Nakamura, Yosio, 2005. Farside deep moonquakes and deep interior of the moon. J. Geophys. Res. 110, E01001 https://doi.org/10.1029/2004JE002332.
Nakamura, Yosio, Latham, Gary V., et al., 1979. Shallow moonquakes: depth, distribution and implications as to the present state of the lunar interior, proc. Lunar Planet Sci, Conf. 10, 2299–2309 (Bib Code: 1979LPSC, 10.2299N).
Nakamura, Yosio, Latham, Gary V., et al., 1982. Apollo lunar seismic experiment-final summary, Proceedings of the thirteenth lunar and planetary science conference, Part 1. J. Geophys. Res. 87, A117–A123.
Nikolaj, L., Dahmen, Clinton, John F., et al., 2021. Super high frequency events: a new class of events recorded by the insight seismometers on mars. JGR Planets. https://doi.org/10.1029/2020JE006599.
Nunn, Ceri, Garcia, Raphel F., et al., 2020. Lunar seismology: a data and instrumentation review. Space Sci. Rev. 216, 89. https://doi.org/10.1007/s1 1214-020-00709-3.
Oberst, Jurgen, Nakamura, Yosio, 1987. Distinct meteoroid families identified on the lunar seismograms, proceedings of the seventeenth lunar and planetary science conference, part 2. J. Geophys. Res. 92 (84), E769–E773.
Robert, L., Kovach, Watkins, Joel S., Talwani, Pradeep, 2024. Apollo 17 Preliminary Science Report.
Sanfomaliti, L.V.K., Zubkova, V.M., et al., 1982. Microseisms at the Venera 13 and Venera 14 landing sites. Sov. Aston. Lett. 8 (4), 0360-0327/82/040241-02.
Shanmugam, M., Vadawale, S.V., et al., 2020. Alpha particle X-ray spectrometer onboard Chandryaan-2 rover. Curr. Sci. 118 (1), 10.